THE JOURNAL OF PHYSICAL CHEMISTRY C
A JOURNAL OF THE AMERICAN CHEMICAL SOCIETY

pubs.acs.org/JPCC
Article

Reactivity of Pentamethylcyclopentenyl Cations toward Olefin Formation in the Methanol-to-Olefin (MTO) Process

Héctor Vicente,* Philipp Huber, Ana G. Gayubo, Felix Studt, and Philipp N. Plessow*

Cite This: J. Phys. Chem. C 2025, 129, 20971−20980
Read Online

ACCESS | Metrics & More | Article Recommendations | Supporting Information

ABSTRACT: Polymethylcyclopentenyl cations are frequently observed experimentally in zeolite catalysis but are investigated to a lesser extent than aromatics or acyclic olefins. Here, the reactivity of the pentamethylcyclopentenyl cation (pentaMCP+) for the formation of olefins in H-SSZ-13 is investigated by using density functional theory (DFT). We find that pentaMCP+ can react similarly to aromatics in the side-chain mechanism with a selectivity for ethylene. The selectivity is due to a specific transition state that favors the elimination of ethylene over the further methylation steps. Generally, our calculations indicate that methylation of the unsaturated side chain is rate-limiting, as also observed for the aromatic cycle. This is because the formation of the neutral species with an unsaturated side chain from the more stable cationic resting state of the hydrocarbon is already unfavorable and adds to the intrinsic barrier for methylation. To estimate the catalytic activity, microkinetic modeling is performed based on the computed Gibbs free energies. Analogous to the aromatic cycle, we find that a second accessible acid site can lower the overall barriers by making stepwise methylation more favorable. Based on our findings, we suggest that there is a third catalytic cycle operating during MTO conversion that is located between the olefin and aromatic cycle and produces primarily ethylene with overall free energy barriers comparable to those of the olefin and aromatic cycle.

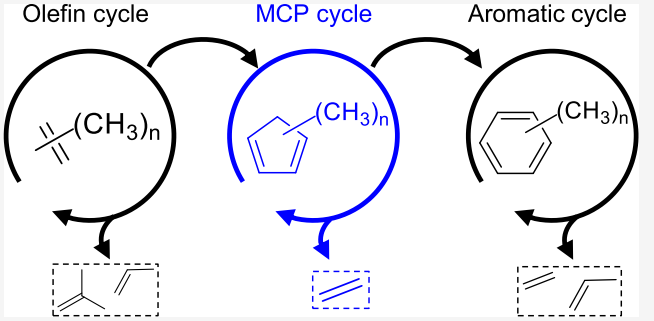

INTRODUCTION

The methanol-to-olefin (MTO) reaction is a widely studied process that can provide a resourceful technology for the energy transition, allowing for the production of a wide range of hydrocarbons (from olefins to gasolines or aromatics) from methanol under mild conditions and by means of acidic zeolites.[1−6] Provided that methanol is produced in a sustainable way by CO or CO_2 hydrogenation, it can be a suitable tool to lower current emissions and in the future decouple the petrochemical industry from oil dependence.[7−9] The MTO process is governed by fast autocatalytic reactions between the methanol feed and the hydrocarbons in the reaction medium that build up the hydrocarbon pool,[10−12] where hydrocarbons act as cocatalysts[6,13,14] Several mechanisms have been developed to describe these reactions, the most accepted being the dual-cycle mechanism. This mechanism comprises two interconnected cycles: (1) the olefin cycle that describes olefin growth through methylation and olefin cracking reactions, and (2) the aromatic cycle, which describes the methylation of aromatic molecules into highly methylated aromatics and the elimination of olefins thereof.[15−17] The two cycles are connected by hydrogen transfer reactions of olefins,[18−20] which yield polyenes that can then form cyclic hydrocarbons and ultimately aromatics.[21] Understanding how these cycles behave and which products they yield is essential to control aspects such as product selectivity or catalyst lifetime, which is mostly affected by the formation of coke from overmethylation of aromatic molecules.[22−25] Atomistic simulations are increasingly used to gain insight into the reactivity of zeolites.[26−29]

Investigations have so far focused on the olefin or aromatic cycles and their respective contributions to olefin formation.[5,26,27,30,31] The general consensus is that this is greatly affected by the catalyst used as the zeolite topology limits the size of the aromatic intermediates that can be formed. With this consideration, different proposals of several mechanisms detail olefin formation within the aromatic cycle.[32−38] Polymethylbenzenes are considered the main intermediates present in the most commonly used zeolites.[39−43] The reactivity of cyclic cations related to polymethylbenzenes was also discussed in the frustrated Lewis pair concept.[44,45] For the aromatic cycle, two types of reactivity are discussed, as described by the paring and the side-chain mechanisms.[5] The paring mechanism produces mainly propylene, and the side-

Received: October 23, 2025
Revised: November 4, 2025
Accepted: November 5, 2025
Published: November 13, 2025

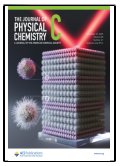

chain mechanism mainly ethylene. This means that regulating the activity of these cycles would allow tuning of product selectivity toward one olefin over the other. Ultimately, this can be achieved with the choice of the zeolite, which has already been proven to have an impact on the ethylene to propylene ratio.[46] For example, the CHA zeolite, which possesses a structure with narrow pores (3.8 × 3.8 Å) with large interior cavities (12.7 × 9.7 Å), can have between 0.8 and 1.0 ethylene to propylene ratio.[47] Meanwhile, MFI zeolites, which have wider pores (of 5.3 × 5.6 Å and 5.1 × 5.5 Å) without cavities, can have ethylene to propylene ratios of less than 0.5.[48]

Early proposals for the paring mechanism involve the antiaromatic pentamethylcyclopentadiene cation, and DFT calculations on this mechanism predicted high overall Gibbs free energy barriers >200 kJ mol^{-1}.[49−51] More recently, a revised paring mechanism was identified through extensive calculations by us[17,52] as well as Wang and co-workers.[53] This mechanism avoids the antiaromatic intermediate, leading to much lower overall Gibbs free barriers on the order of 150 kJ mol^{-1}. Similarly, for the aromatic side-chain mechanism, high barriers have been computed, owing to the instability of the intermediate that needs to be methylated, which is hexamethylmethylenecyclohexadiene (HMMC), when starting from the heptamethylbenzylium cation (heptaMB+).[37,54−57] Here we have shown recently for H-SSZ-13 that an accessible second site makes the side-chain mechanism more favorable by lowering the barrier for stepwise methylation.[58]

Aside from acyclic olefins and aromatics, polymethylcyclopentenyl cations (MCP+) have been detected with different techniques, such as nuclear magnetic resonance (NMR)[59−62] or ultraviolet or infrared spectroscopy,[63−66] and in several zeolites typically used for the MTO reaction like H-ZSM-5 or H-ZSM-22,[61,67−69] H-SSZ-13,[60,70] or SAPO catalysts.[71,72] A side-chain mechanism analogous to the aromatic cycle was investigated for the pentamethylcyclopentenyl cation (pentaMCP+), where methylation itself was found to be the rate-limiting step with an energetic span[73] (Gibbs free energy) of 180 kJ mol^{-1} at 300 °C for H-RUB-50[74] and 218 kJ mol^{-1} at 400 °C for H-SAPO-34.[75] This translates into rather low turnover frequency (TOF) values of 5 × 10^{-4} s^{-1} and 1.7 × 10^{-4} s^{-1}, respectively.

In this work, we investigate the reactivity of the pentaMCP+ intermediate by using density functional theory calculations and microkinetic modeling. A mechanism analogous to the side-chain mechanism of the aromatic cycle is studied for both ethylene and propylene formation. In addition to concerted methylation on a single acid site, stepwise methylation on two acid sites is considered. By doing so, we shed light on the existence of a third catalytic cycle based on MCP+ operating alongside the olefin and aromatic cycle.

METHODS

The mechanism was investigated for the H-SSZ-13 zeolite, which crystallizes in the chabazite (CHA) structure and contains a single T-site. We used a model with one acid site per 36T-unit cell for the single-site CHA calculations and two acid sites per two unit cells for the second-site-assisted calculations with a Si/Al ratio of 35 in both cases. The lattice constants were $a = b = 13.625$ Å and $c = 15.067$ Å[17] for the CHA structure, and a (2 × 1 × 1) CHA supercell was used for the dual site structure. The two sites are separated by three SiO units with a distance of about 9 Å, as in a previous work,[58] which allows protonation/deprotonation of the adsorbed molecule without significant rotation and reorientation inside the cavity. All structures were optimized using periodic density functional theory (DFT) with the dispersion corrected PBE-D3 functional,[76,77] with the projector-augmented wave (PAW) method as implemented in the Vienna Ab Initio Simulation Package (VASP), in version 6.4.3.[78,79] For every calculation, standard PAW potentials[80] and a plane-wave basis set with an energy cutoff of 400 eV for the wave function were used with a convergence criterion of 0.001 eV $Å^{-1}$, Gaussian smearing with a width of 0.1 eV, and k-point sampling only at the Γ-point. For the most important intermediates and transition states, different starting points for the optimizations were created manually, starting from those previously studied for the side-chain mechanism with heptaMB+ and other similar systems.[57,58,81−85] Transition states were calculated using the automated relaxed potential surface scans (ARPESS) method,[86] and we verified the existence of a single imaginary frequency. Vibrational analysis was performed by calculating a partial Hessian of the adsorbate atoms and the acid site, consisting of the aluminum atom and all adjacent oxygen and silicon atoms (four oxygen and silicon atoms for each active site), with an atomic displacement of 0.01 Å. Distortion along the transition mode, followed by optimization toward the end points, led to the corresponding reactants and products.

DFT calculations with PBE-D3 can underestimate energy barriers by up to 50 kJ mol^{-1},[87−89] and we therefore performed additional single-point calculations with the ωB97M functional[90] with D4-corrections[91,92] (ωB97M-D4), as implemented in a local VASP version. In a recent study, we benchmarked this functional alongside many others[88] and we concluded that, when evaluating hydrocarbon reactions in zeolites, it provided an accurate approximation to other high-level ab initio methods, with mean absolute errors below 8 kJ mol^{-1} and at a much lower computational cost.

Steady-state mean-field microkinetic modeling was carried out using the surfprobe program of the DETCHEM software package,[93] at a partial pressure of methanol of 1 bar, and an initial active site coverage of 1 mol cm^{-2}. Steady-state rates were extracted after a simulation time of 10^5 s and were then used to compute the turnover frequency (TOF). The input files used for the surfprobe program of the DETCHEM software are provided as Supporting Information. The coverage of every intermediate state for both models is presented in Table S9.

RESULTS AND DISCUSSION

Several MCP+ have been observed experimentally, depending on the zeolite framework used.[67,69,74] For this study, we chose the H-SSZ-13 zeolite due to the simplicity of the CHA framework, with only one T-site, and for comparison with other mechanisms previously computed for this system. The chabazite framework is known to accommodate large adsorbates, up to heptaMB+, in the aromatic cycle. For H-SSZ-13, pentaMCP+ was found as the main polymethylcyclopentenyl cation species present during MTO.[60,69] For H-SAPO-34, which also crystallizes in the chabazite framework, pentaMCP+ was also identified, alongside the heptamethylcyclopentenyl cation (heptaMCP+).[72] We chose to investigate pentaMCP+ also because of its high symmetry, which leads to fewer possible isomers.

Similar to the study in ref 74, we investigated a mechanism resembling the side-chain mechanism of the aromatic cycle. As

https://doi.org/10.1021/acs.jpcc.5c07265
J. Phys. Chem. C 2025, 129, 20971−20980

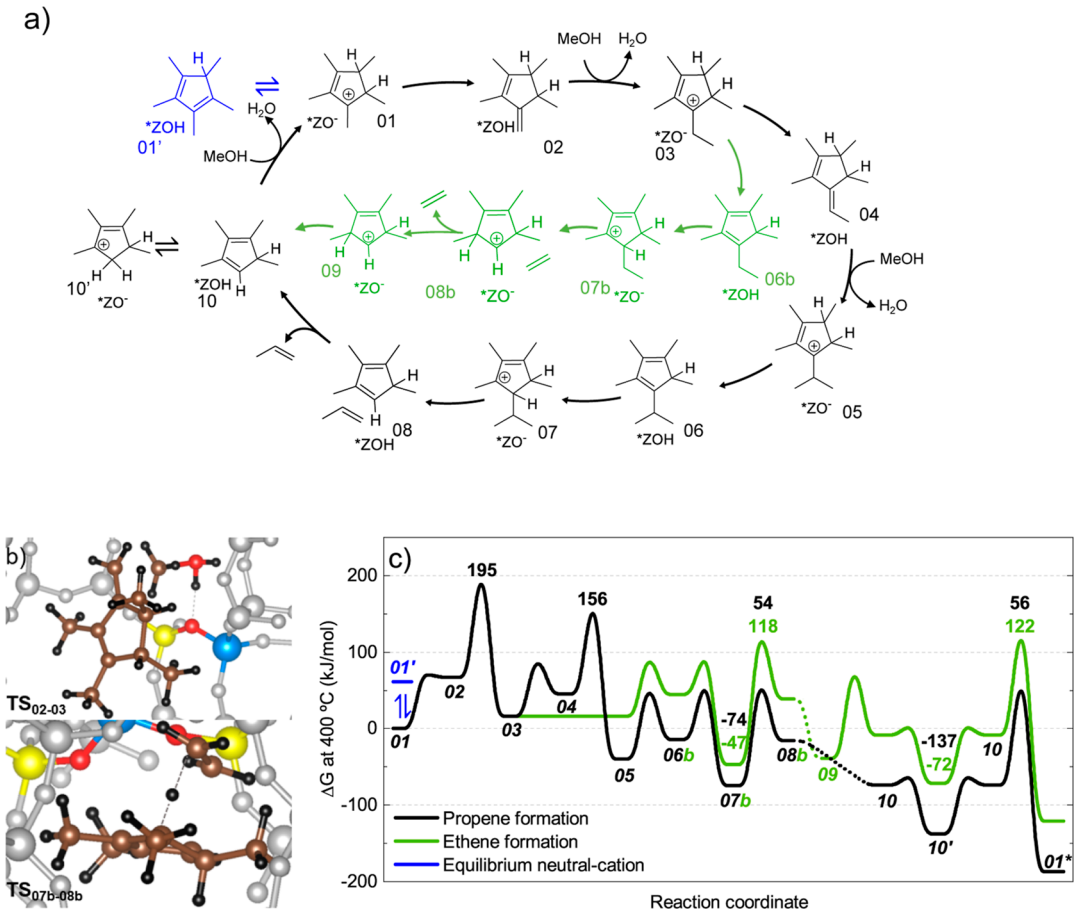

Figure 1. (a) Overview of the proposed pentaMCP+ cycle for propylene and ethylene formation, (b) methylation (TS_{02-03}) and ethylene formation ($TS_{07b-08b}$) steps, and (c) Gibbs free energy diagram of the pentaMCP+ cycle mechanism proposed for propylene and ethylene formation at 400 °C and 1 bar with the ωB97M-D4 functional. All shown free energy values are given relative to structure *01*. Color code for the atomic structures of the key transition states in (b): blue = Al, yellow = Si, red = O, brown = C, black = H, and gray = remaining framework.

shown in Figure 1a, we start from the neutral tetramethylcyclopentadiene (01′), which is easily protonated to the more stable pentaMCP+ with a moderate barrier of 129 kJ mol^{-1}. We find pentaMCP+ to be more stable than neutral pentaMCP by 62 kJ mol^{-1}. Deprotonation of a methyl group yields a methylene group (02), which can subsequently be methylated to an ethyl side chain. This is analogous to the side-chain mechanism, where, starting from hexamethylbenzene (hexaMB), methylation gives heptaMB+ and subsequent deprotonation gives hexamethylmethylenecyclohexadiene (HMMC). In the aromatic cycle, creation of a cation such as heptaMB+ from the neutral aromatic species is less favorable due to the loss of aromaticity. For example, we found a formation free energy of $\Delta G = -14$ kJ mol^{-1} of heptaMB+ from hexaMB in ref 55.

The central and most problematic step is the methylation of the methylene side chain, which requires a barrier of 195 kJ mol^{-1}. This relatively high barrier is mainly due to the fact that the reactant (02) is relatively unstable, being 67 kJ mol^{-1} less stable than pentaMCP+. The methylation barrier (02−03) relative to species 02 is 128 kJ mol^{-1}. For the aromatic cycle, we found the neutral intermediate HMMC to be less stable than heptaMB+ by 84 kJ mol^{-1},[55] with a similar intrinsic barrier (121 kJ mol^{-1} relative to HMMC), while the apparent barrier relative to heptaMB+ was 206 kJ mol^{-1}. We thus find that side-chain methylation is similar to the aromatic cycle but requires slightly lower barriers since the neutral species with the methylene group (02) is more stable than the corresponding species (HMMC) in the aromatic cycle.

In the hexaMB-based aromatic cycle, elimination of ethylene occurs after several methyl shifts that bring a methyl group into a geminal position to the ethyl side chain. The eliminated ethyl cation is immediately deprotonated by the zeolite to produce the neutral acid site, ethylene, and hexaMB. This mechanism benefits from producing a neutral, stable aromatic molecule and proceeds with a low barrier, on the order of 100 kJ mol^{-1}.[55]

For the pentaMCP+ based cycle, elimination of ethylene occurs after several protonation/deprotonation steps that bring a proton into a geminal position to the ethyl group. In this case, as opposed to the hexaMB cycle, formation of a neutral pentaMCP is less favorable (barrier 190 kJ mol^{-1}), and elimination of ethylene thus proceeds in a different manner, with $TS_{07b-08b}$, see Figure 1b. After elimination of the intermediate ethyl cation, it is instead directly deprotonated by intermediate tetraMCP to form tetraMCP+ and neutral ethylene. The barrier for ethylene elimination is still relatively high compared to propene elimination, with 165 kJ mol^{-1}.

Propylene formation requires a second methylation step, which comes after deprotonation of the ethyl side chain. The Gibbs free energy diagram in Figure 1c seems to imply that the formation of species 04 and its methylation could proceed with

https://doi.org/10.1021/acs.jpcc.5c07265
J. Phys. Chem. C 2025, 129, 20971−20980

a low barrier. However, species 03 will quickly react to form the more stable isomer 07b. Relative to 07b, the second side-chain methylation barrier 04−05, which generates the isopropyl side chain, is 204 kJ mol^{-1}. Same as for the aromatic side-chain mechanism, the second methylation step is thus unfavorable, giving a preference to ethylene formation.

As opposed to ethylene formation, propylene formation occurs in a similar manner as in the aromatic cycle; i.e., the proton is transferred from the intermediate isopropyl cation to the zeolite, not to the hydrocarbon. The main difference is that here it is more favorable to have a hydrogen in the geminal position than to have the isopropyl group, in contrast to a methyl group in the aromatic cycle. We also tested the intramolecular proton transfer proposed for ethylene elimination for the corresponding elimination of propylene, obtaining a barrier 10 kJ mol^{-1} higher. For propylene, both types of elimination thus proceed with low barriers.

The methylation of neutral tetraMCP via TS_{10-01} yields pentaMCP+ with a relatively low intrinsic barrier of 130 kJ mol^{-1}. However, as depicted in Figure 1a, the neutral tetraMCP can easily be protonated to form the more stable tetraMCP+ isomer (10′). The barrier for the methylation of neutral tetraMCP to pentaMCP+ relative to tetraMCP+ is 194 kJ mol^{-1}, which is almost identical to the first methylation step.

With relatively high barriers of about 195 kJ mol^{-1}, the resulting TOFs are ≲0.01 s^{-1}, as we will discuss in more detail later. In our previous work,[58] we have shown that the presence of a second acid site in the cavity of H-SSZ-13 can lower the methylation barrier for the aromatic side-chain mechanism, if it proceeds via a surface methoxy species (SMS). Usually, direct methylation is more favorable for HMMC in the aromatic cycle. Stepwise or dissociative methylation proceeds via the creation of an SMS from methanol in the first step, while the SMS is then transferred to the substrate (HMMC) in a second step. The first step also suffers from the trivial issue that HMMC is rather unstable, and SMS formation would be much more favorable if it could occur in the presence of the more stable heptaMB+. This, however, is not possible since in the presence of the cationic adsorbate, the acid site is anionic. A second acid site in the same cavity allows for resolving this, as one site can form the stable zwitterion (cationic adsorbate and anionic site), while the other site forms an SMS. In principle, this introduces no specific constraints on the location of the second site other than that it has to be in the same cavity. For computational convenience, the location of the second site was chosen such that it can interact with the adsorbate without the need for excessive rotations and rearrangements of the adsorbate in the cavity.[58] For the side-chain mechanism of the aromatic cycle within the dual-site model, involvement of the second acid site was previously found to lower the barrier from 205 kJ mol^{-1} (concerted methylation) to 168 kJ mol^{-1} (stepwise methylation).[58]

We have investigated the effect of a second acid site in the pentaMCP+ cycle discussed above, using the same model as in ref 58. The model is shown in Figure 2 and employs a supercell with 72 T atoms, thus maintaining the Si/Al ratio of 35. Figure 3 shows both the mechanism and the corresponding Gibbs free energy diagram. The states of the two acid sites (ZOH, ZOMe, and ZO$^-$) are indicated below the adsorbate. As in the single-site mechanism, all Gibbs free energies are referenced to the starting point pentaMCP+ (01). With the first acid site in an anionic state, SMS can be created at the second site with a moderate barrier of 153 kJ mol^{-1}. From that SMS, side-chain

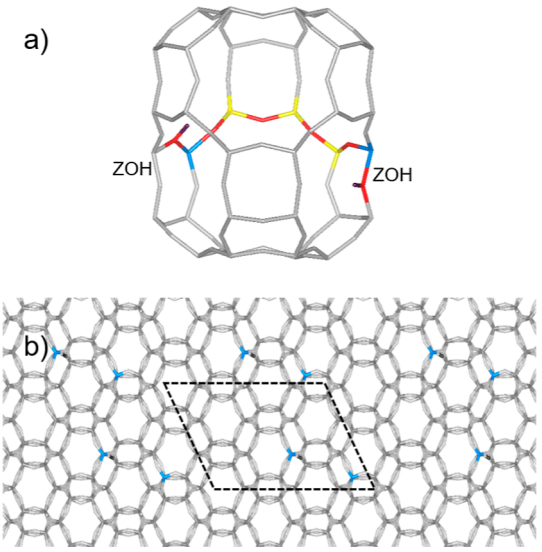

Figure 2. Structural model of the double-site CHA supercell with (a) the cavity including the two Al atoms and (b) top view of the supercell.

methylation proceeds (coincidentally) also with a barrier of 153 kJ mol^{-1} (referred to the more stable 01_S intermediate), followed by deprotonation/protonation up to 07b, which is the most stable intermediate observed also in the single-site mechanism. Then, the second SMS formation occurs with a barrier slightly lower than that of the first one (141 kJ mol^{-1}).

After the second SMS formation, ethylene is eliminated with a barrier of 134 kJ mol^{-1}, which is 31 kJ mol^{-1} lower than that with a single site. Subsequently, the second SMS methylates tetraMCP to pentaMCP+ (TS_{10-01}) with a barrier lower than that for the first methylation (148 kJ mol^{-1}). Again, this barrier is referenced to the highly stable tetraMCP+ formed by protonation of the neutral tetraMCP. For ethylene formation, the highest barriers are thus those for methylation (153 kJ mol^{-1}), while elimination requires lower barriers (134 kJ mol^{-1}).

The second SMS can also methylate the ethylene group, forming the isopropyl side chain. This step has a barrier of 156 kJ mol^{-1}, relative to 07b. Propylene elimination occurs analogously to the single-site mechanism, with a barrier of 147 kJ mol^{-1} relative to 07_S. For propylene formation, the barriers for methylation (153 kJ mol^{-1}) and elimination (156 kJ mol^{-1}) are thus similar.

Overall, the second site reduces the highest barrier from about 195 to around ≲156 kJ mol^{-1}. For the single site, the selectivity is determined by the barriers of the methylation of the ethylene side chain (TS_{04-05}) relative to 07b (204 kJ mol^{-1}) versus ethylene elimination ($TS_{07b-08b}$) relative to 07b (165 kJ mol^{-1}). For the dual site case, the selectivity is determined by the barriers of TS_{04-05} relative to 07b (156 kJ mol^{-1}) versus TS_{07b_S-08b} relative to 07b (134 kJ mol^{-1}). The selectivity for ethylene thus remains but is less pronounced for the dual site case when analyzing only the barriers.

It is obvious from Figure 3c that there are multiple barriers in a similar range. Given that the reaction path furthermore splits into two branches, we performed microkinetic modeling to determine the activity as given by the turnover frequency (TOF) and also the selectivity for ethylene and propylene. The main results for the microkinetic analysis are shown in Table 1.

https://doi.org/10.1021/acs.jpcc.5c07265
J. Phys. Chem. C 2025, 129, 20971−20980

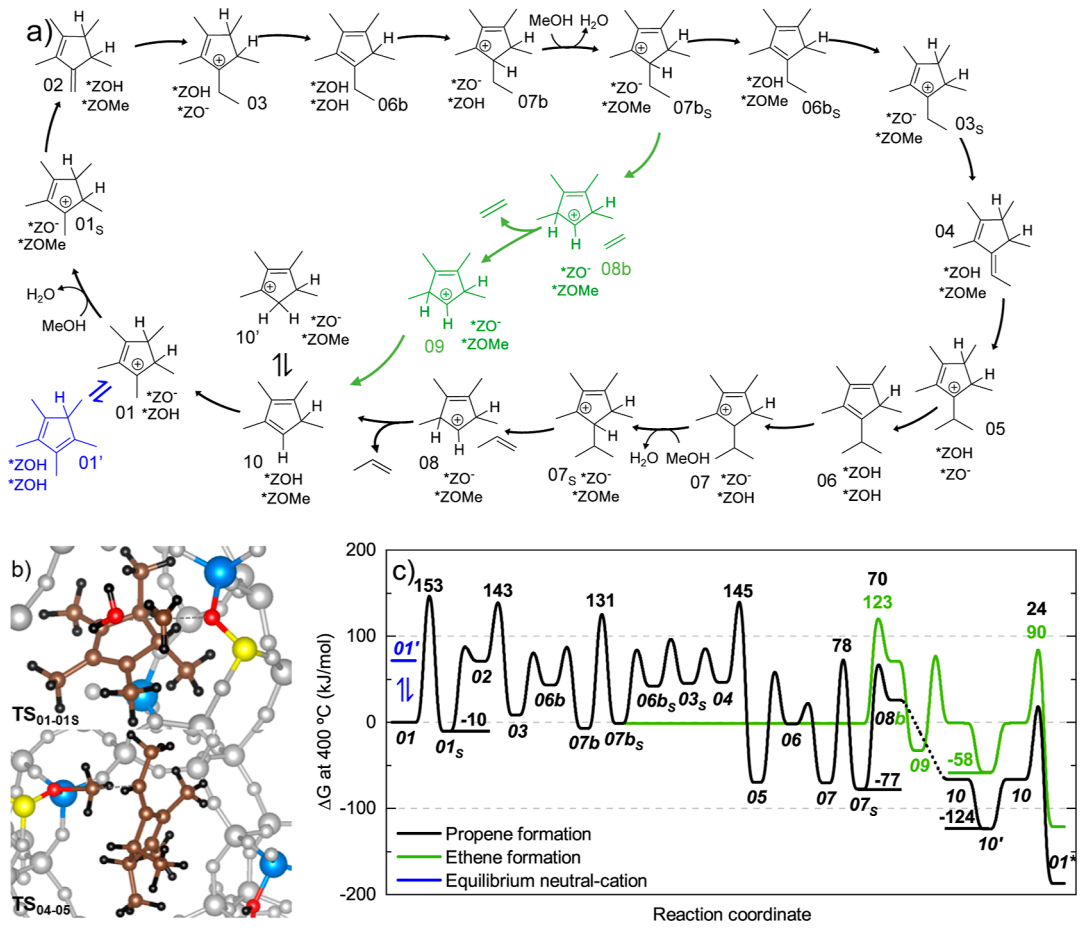

Figure 3. (a) Overview of the proposed pentaMCP+ cycle for propylene and ethylene formation assisted by a second acid site, (b) SMS formation (TS_{01-01_S}) and second methylation (TS_{04-05}) steps, and (c) Gibbs free energy diagram of the pentaMCP+ cycle mechanism assisted by a second acid site proposed for propylene and ethylene formation at 400 °C and 1 bar with ωB97M-D4. All shown free energy values are given relative to structure *01*.

Table 1. Free Energy Barriers and Coverages for the Rate-Determining Steps in the Two Variants of the PentaMCP+ Mechanism (Propylene and Ethylene Formation) for the Single Site and the Second Site-Assisted System and TOFs for the Complete Mechanism[a]

	single site	second site-assisted
	Microkinetic Model	
coverage	01: 54%	01: 39%
	10′: 46%	01_S: 42%
		07b: 3%
		10′: 15%
TOF C_3H_6 (s^{-1})	5.8×10^{-6}	1.4×10^{-1}
TOF C_2H_4 (s^{-1})	5.9×10^{-3}	6.9×10^{0}
[b]selectivity C_2H_4	98%	98%
	Energetic Span Model	
TOF C_2H_4 (s^{-1})	[c]1.1×10^{-2}	[d]1.8×10^{1}
[b]selectivity C_2H_4	[e]100%	[f]98%

[a]Values calculated using microkinetic modelling at 400 °C and at a reference pressure of 1 bar. [b]Selectivity calculated as $TOF_{C_2H_4}/(TOF_{C_2H_4} + TOF_{C_3H_6})$. [c]$G(TS_{02-03}) - G(01) = 195$ kJ mol^{-1}. [d]$G(TS_{04-05}) - G(01_S) = 156$ kJ mol^{-1}. [e]Difference in barriers 39 kJ mol^{-1}. [f]Difference in barriers 22 kJ mol^{-1}.

For ethylene formation at the single site, the microkinetic model predicts a TOF of 5.9×10^{-3} s^{-1} and a selectivity of 98% for ethylene. This agrees reasonably well with a simpler analysis as described by the energetic span model,[73] according to

$$r = \frac{k_B T}{h} e^{-\frac{\Delta G}{k_B T}} \quad (1)$$

which also predicts a high selectivity (100%) and an activity about two times larger. The main barrier that hinders the reaction in the single site configuration is S_{02-03}, being 195 kJ mol^{-1} above the most stable state before that, which is structure 01. This high barrier prevents the reaction from progressing forward, as shown by the high steady state coverage of 54% for θ_{01}. Afterward, the reaction quickly progresses to intermediate 10′, with $\theta_{10'}$ = 46%, from which the second large barrier for the methylation of structure 10 to regain 01 needs to be overcome. In addition, the propylene formation in the single site has another high barrier ($G(TS_{04-05}) - G(07b) = 204$ kJ mol^{-1}), higher than that of TS_{02-03}, which explains the higher selectivity obtained for ethylene.

As expected, given the overall lower barriers, the microkinetic model with two sites gives higher TOF values for both olefins. Despite the TOF increase, selectivity remains the same, with an ethylene selectivity value of 98%. Two of the largest free energy barriers correspond to the formation of the first SMS (TS_{01-01_S}) and methylation via this SMS (TS_{02-03}).

https://doi.org/10.1021/acs.jpcc.5c07265
J. Phys. Chem. C 2025, 129, 20971−20980

Therefore, the steady-state coverage corresponds mostly to structures 01 and 01_S, with values of θ_{01} = 39% and θ_{01_S} = 42%, respectively. After these steps, the mechanism for ethylene formation presents barriers 20 kJ mol^{-1} lower until ethylene formation. Then structure 10′ is reached without any significant barrier, with a coverage of 15%, and has to overcome a moderate barrier of 148 kJ mol^{-1} for reaching structure 01 again. Once again, the propylene pathway is less selective due to the second methylation barrier (TS_{04-05}), which has the highest barrier of the mechanism with 156 kJ mol^{-1} relative to the most stable previous intermediate 01_S. This is 22 kJ mol^{-1} higher than the ethylene formation barrier (134 kJ mol^{-1}), resulting in a lower propylene TOF compared to that for ethylene.

We will now compare the activity of the pentaMCP+ based cycle to the aromatic and olefin cycles for H-SSZ-13. This comparison is based on an analysis of rate-limiting steps according to the energetic span model,[73] and we note that this approach only describes the intrinsic reactivity of the corresponding mechanisms per active site. Other effects, such as diffusion limitations, actual coverages, and partial pressures, are not included. Besides the barriers of a cycle (olefin, aromatic, or MCP+), it is of course also important to what extent these species are present. This includes not only the aspect of formation but also that both aromatics and MCP+ are trapped in the cavities of chabazite. Due to the limited space in a cavity, the presence of an aromatic molecule or MCP+ can then be expected to block the corresponding sites and effectively suppress the other cycles.

Again, we stress that the methylbenzenes (6 π-electrons) and their associated cations (4 π-electrons) have one more unsaturated bond than methylcyclopentadienes (4 π-electrons) and methylcyclopentenyl cations (2 π-electrons). These species can therefore not be expected to be in a rapid equilibrium. To allow direct comparison, barriers previously computed with ab initio methods on cluster models[58] were for this work recomputed with ωB97M-D4 single points on the already existing optimized periodic structures. The comparison of the rate-determining barriers with ωB97M-D4 and ab initio calculations is summarized in Table 2, showing that ωB97M-D4 generally gives somewhat higher barriers for the aromatic cycle than those obtained previously with ab initio methods. For the side-chain mechanism, we have previously reported barriers of 167 and 168 kJ mol^{-1} (relative to heptaMB+) for the first and second steps of the stepwise methylation of HMMC, when assisted by a second site. The barrier for the first step agrees well (166 kJ mol^{-1} with ωB97M-D4) and is not listed in Table 2. The barrier for the second step, however, is higher, with 192 kJ mol^{-1}. This overestimation by 24 kJ mol^{-1} is to a large extent due to the fact that HMMC relative to heptaMB+ is too high in free energy by 12 kJ mol^{-1} with ωB97M-D4. For the paring mechanism, we have previously recomputed the highest barriers from our initial study on a single site,[17] in our subsequent study on two sites.[58] The highest barriers obtained for the two alternative pathways in those studies, labeled TS_{5-6r} and TS_{6-7}, were reported to be both 157 kJ mol^{-1} for the two-site-assisted case.[58] The barriers for TS_{5-6r} and TS_{6-7} recomputed with ωB97M-D4 are 179 and 165 kJ mol^{-1}, respectively. While one of the barriers is 22 kJ mol^{-1} higher, the other is similar, overall agreeing with the analysis that the paring mechanism is expected to be active. For the olefin cycle, cracking becomes more favorable when stable intermediate cations can be formed,[94] meaning cracking becomes facile for heavy olefins.[95] Methylation of light olefins, which multiple investigations have found to occur via the stepwise (dissociative) mechanism at high temperatures, presents higher barriers.[96,97] The rate-limiting step is then the formation of the SMS intermediate in this dissociative methylation, which we recomputed in the dual-site model for consistency with a barrier of 154 kJ mol^{-1}. While the accuracy of ωB97M-D4 is in these cases somewhat less than anticipated based on ref 88, we still believe that the accuracy is sufficient for most cases, without extreme outliers, and is justified by the savings in computational time and the benefit of using only periodic models.

Overall, we find the barriers for the pentaMCP+ based side-chain mechanism to be around 160 kJ mol^{-1} and thus similar or even lower than results obtained for the paring and side-chain mechanism. This indicates that, if MCP+ species are present in the catalytic pool of species, the MCP+ cycle could be faster than the aromatic cycle for the case of H-SSZ-13. Based on the degree of oxidation of the olefins, we would expect MCP+ species as a likely intermediate between olefins and aromatics, such that they are eventually oxidized to aromatics through hydrogen transfer reactions.

Table 2. Comparison of the Different Cycles of the Hydrocarbon Pool Based on Rate-Determining Gibbs Free Energy Barriers According to the Energetic Span Model[a]

cycle	barrier	ωB97M-D4	ab initio[b]
olefin	SMS formation	154	-
aromatic, paring	TS(6−7)	165	157
aromatic, side chain	TS(3s−4s)	192	168
MCP+, side chain	TS(02−03)	153	-

[a]All data are for H-SSZ-13 at 400 °C and 1 bar reference pressure and use the dual-site model for consistency. For transition states from previous work, we use the same labels defined therein.[58] [b]Ref 58.

SUMMARY AND CONCLUSION

The reactivity of the pentamethylcyclopentenyl cation (pentaMCP+) for the production of olefins has been investigated by using density functional theory and microkinetic modeling using H-SSZ-13 as the catalyst. Our investigations identified pentamethylcyclopentadiene and its protonated form pentaMCP+ as key intermediates that are structurally similar to both olefins as well as to aromatics and their protonated forms, such as hexaMB and heptaMB+. The most favorable reactivity of pentaMCP+ resembles the side-chain mechanism of the aromatic cycle. After an unsaturated methylene side chain is formed, it can be methylated to form an ethyl side chain, which can be subsequently eliminated as ethylene. Importantly, this elimination is more favorable than further methylation, resulting in a high selectivity for ethylene. As in other studies on the side-chain mechanism of the aromatic cycle, we find a high barrier for concerted methylation of the methylene side chain, here 194 kJ mol^{-1}. This is because, starting from the most stable cationic species (here, pentaMCP+, for aromatics, for example, heptaMB+), creation of the neutral species to be methylated is uphill in free energy by >50 kJ mol^{-1}, which adds to the intrinsic barrier for methylation. As in a previous investigation, we find that the (otherwise unfavorable) stepwise methylation mechanism in combination with a second accessible acid site allows us to circumvent this problem. This is because the first step of

https://doi.org/10.1021/acs.jpcc.5c07265
J. Phys. Chem. C 2025, 129, 20971−20980

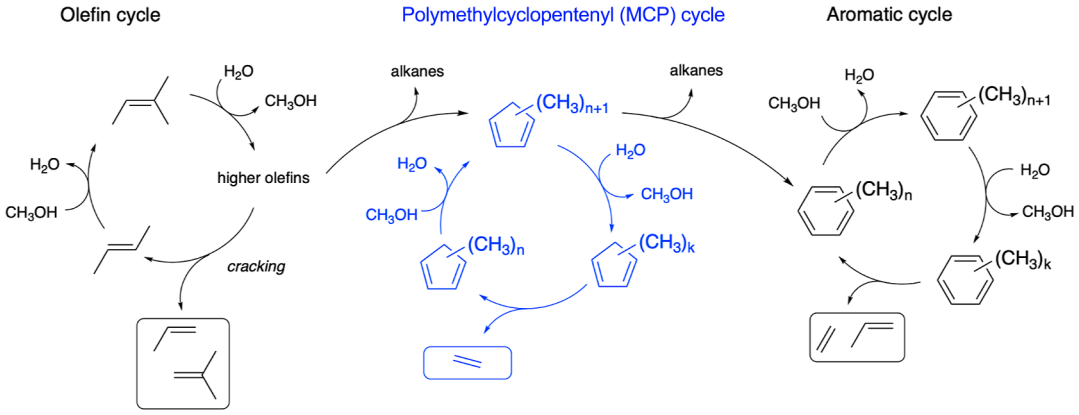

Figure 4. Schematic overview of the olefin cycle, the MCP cycle, and the aromatic cycle.

stepwise methylation, turning the first site into an SMS, can occur with the hydrocarbon in the more stable cationic state if the negative charge is on the second site. In our investigation, this lowers the highest barrier from 195 kJ mol^{-1} to 153 kJ mol^{-1}, making this mechanism thus much more facile. These low barriers suggest high catalytic activity of the MCP cycle for ethylene formation, which is corroborated by microkinetic modeling, which predicts a TOF of 6.9 s^{-1}. This is in contrast to high DFT barriers reported previously for the reactivity of MCP+.[74,75]

Importantly, the overall barrier of the MCP+ cycle is therefore 153 kJ mol^{-1} for the production of ethylene. Our investigations therefore shed light on this third catalytic cycle, which we term the MCP cycle, and which runs alongside the well-known olefin and aromatic cycles (see Figure 4), with barriers that are similar or lower than either of them (see Table 2).

However, the extent to which the MCP cycle contributes to overall production rates of olefins greatly depends on the existence of MCP+ species during the reaction and, thus, the formation rates of these cationic species from olefins and depletion rates through further reaction toward aromatics. Nevertheless, our results show a clear predominance of the MCP cycle toward ethylene formation over propylene. Suppressing the formation and catalytic activity of MCP+ species is therefore expected to reduce ethylene formation via the investigated side-chain mechanism. Additionally, low free energy barriers were obtained only with the presence of two accessible sites, which suggests that another way of avoiding this reactivity would be to control the distribution of the acid sites. These questions need extensive experimental and theoretical studies to answer but might hold the key to improve not only activity and selectivity but also the lifetime of zeotype catalysts.

■ ASSOCIATED CONTENT

Supporting Information

The Supporting Information is available free of charge at https://pubs.acs.org/doi/10.1021/acs.jpcc.5c07265.

Total energies, Cartesian coordinates, and further analysis (PDF)

(ZIP)

■ AUTHOR INFORMATION

Corresponding Authors

Héctor Vicente − *Department of Chemical Engineering, University of the Basque Country, Leioa 48940, Spain; Institute of Catalysis Research and Technology, Karlsruhe Institute of Technology, Eggenstein-Leopoldshafen 76344, Germany;* orcid.org/0000-0001-9166-9743; Email: hector.vicente@ehu.eus

Philipp N. Plessow − *Institute of Catalysis Research and Technology, Karlsruhe Institute of Technology, Eggenstein-Leopoldshafen 76344, Germany;* orcid.org/0000-0001-9913-4049; Email: plessow@kit.edu

Authors

Philipp Huber − *Institute of Catalysis Research and Technology, Karlsruhe Institute of Technology, Eggenstein-Leopoldshafen 76344, Germany*

Ana G. Gayubo − *Department of Chemical Engineering, University of the Basque Country, Leioa 48940, Spain*

Felix Studt − *Institute of Catalysis Research and Technology, Karlsruhe Institute of Technology, Eggenstein-Leopoldshafen 76344, Germany; Institute for Chemical Technology and Polymer Chemistry, Karlsruhe Institute of Technology, Karlsruhe 76131, Germany;* orcid.org/0000-0001-6841-4232

Complete contact information is available at: https://pubs.acs.org/10.1021/acs.jpcc.5c07265

Notes

The authors declare no competing financial interest.

■ ACKNOWLEDGMENTS

The authors acknowledge support by the state of Baden−Württemberg through bwHPC (bwunicluster and JUSTUS, RV bw17D011) and the German Research Foundation (DFG) through grant no. INST 40/575-1 FUGG (JUSTUS 2 cluster). Financial support from the Helmholtz Association is also gratefully acknowledged. Gefördert durch die Deutsche Forschungsgemeinschaft (DFG) Projektnummer 434253773 is also acknowledged. H.V. is grateful for his postdoctoral grant from the Basque Government (POS_2023_1_0018).

■ REFERENCES

(1) Chang, C. D.; Lang, W. H. Process for manufacturing olefins. U.S. Patent 4,025,576 A, 1977.

(2) Stöcker, M. Methanol-to-hydrocarbons: catalytic materials and their behavior. *Microporous Mesoporous Mater.* **1999**, *29*, 3−48.
(3) Tian, P.; Wei, Y.; Ye, M.; Liu, Z. Methanol to Olefins (MTO): From Fundamentals to Commercialization. *ACS Catal.* **2015**, *5*, 1922−1938.
(4) Lin, S.; Li, H.; Tian, P.; Wei, Y.; Ye, M.; Liu, Z. Methanol to Olefins (MTO): Understanding and Regulating Dynamic Complex Catalysis. *J. Am. Chem. Soc.* **2025**, *147*, 11585−11607.
(5) Olsbye, U.; Svelle, S.; Bjørgen, M.; Beato, P.; Janssens, T. V. W.; Joensen, F.; Bordiga, S.; Lillerud, K. P. Conversion of Methanol to Hydrocarbons: How Zeolite Cavity and Pore Size Controls Product Selectivity. *Angew. Chem., Int. Ed.* **2012**, *51*, 5810−5831.
(6) Olsbye, U.; Svelle, S.; Lillerud, K. P.; Wei, Z. H.; Chen, Y. Y.; Li, J. F.; Wang, J. G.; Fan, W. B. The formation and degradation of active species during methanol conversion over protonated zeotype catalysts. *Chem. Soc. Rev.* **2015**, *44*, 7155−7176.
(7) Olah, G. A. Beyond oil and gas: the methanol economy. *Angew. Chem., Int. Ed. Engl.* **2005**, *44*, 2636−2639.
(8) Olah, G. A. Towards oil independence through renewable methanol chemistry. *Angew. Chem., Int. Ed. Engl.* **2013**, *52*, 104−107.
(9) Etzold, B. J. M.; Hungsberg, M.; Ebrahim-Moghaddam, M.; Herold, F.; Dahmen, N.; Studt, F. Energy Requirements for Sustainable Olefin Production From CO2 via Electro- or Thermal Catalysis. *Chem. Eng. Technol.* **2025**, *48*, No. e70034.
(10) Dahl, I. M.; Kolboe, S. On the Reaction-Mechanism for Propene Formation in the Mto Reaction over Sapo-34. *Catal. Lett.* **1993**, *20*, 329−336.
(11) Dahl, I. M.; Kolboe, S. On the Reaction Mechanism for Hydrocarbon Formation from Methanol over SAPO-34: I. Isotopic Labeling Studies of the Co-Reaction of Ethene and Methanol. *J. Catal.* **1994**, *149*, 458−464.
(12) Dahl, I. M.; Kolboe, S. On the reaction mechanism for hydrocarbon formation from methanol over SAPO-34 0.2. Isotopic labeling studies of the co-reaction of propene and methanol. *J. Catal.* **1996**, *161*, 304−309.
(13) Ilias, S.; Bhan, A. Mechanism of the Catalytic Conversion of Methanol to Hydrocarbons. *ACS Catal.* **2013**, *3*, 18−31.
(14) Yarulina, I.; Chowdhury, A. D.; Meirer, F.; Weckhuysen, B. M.; Gascon, J. Recent trends and fundamental insights in the methanol-to-hydrocarbons process. *Nat. Catal.* **2018**, *1*, 398−411.
(15) Bjorgen, M.; Svelle, S.; Joensen, F.; Nerlov, J.; Kolboe, S.; Bonino, F.; Palumbo, L.; Bordiga, S.; Olsbye, U. Conversion of methanol to hydrocarbons over zeolite H-ZSM-5: On the origin of the olefinic species. *J. Catal.* **2007**, *249*, 195−207.
(16) Svelle, S.; Joensen, F.; Nerlov, J.; Olsbye, U.; Lillerud, K.-P.; Kolboe, S.; Bjørgen, M. Conversion of Methanol into Hydrocarbons over Zeolite H-ZSM-5: Ethene Formation Is Mechanistically Separated from the Formation of Higher Alkenes. *J. Am. Chem. Soc.* **2006**, *128*, 14770−14771.
(17) Plessow, P. N.; Enss, A. E.; Huber, P.; Studt, F. A new mechanistic proposal for the aromatic cycle of the MTO process based on a computational investigation for H-SSZ-13. *Catal. Sci. Technol.* **2022**, *12*, 3516−3523.
(18) Müller, S.; Liu, Y.; Kirchberger, F. M.; Tonigold, M.; Sanchez-Sanchez, M.; Lercher, J. A. Hydrogen Transfer Pathways during Zeolite Catalyzed Methanol Conversion to Hydrocarbons. *J. Am. Chem. Soc.* **2016**, *138*, 15994−16003.
(19) Sun, X.; Mueller, S.; Shi, H.; Haller, G. L.; Sanchez-Sanchez, M.; van Veen, A. C.; Lercher, J. A. On the impact of co-feeding aromatics and olefins for the methanol-to-olefins reaction on HZSM-5. *J. Catal.* **2014**, *314*, 21−31.
(20) Kilburn, L.; DeLuca, M.; Hoffman, A. J.; Patel, S.; Hibbitts, D. Comparing alkene-mediated and formaldehyde-mediated diene formation routes in methanol-to-olefins catalysis in MFI and CHA. *J. Catal.* **2021**, *400*, 124−139.
(21) Montalvo-Castro, H.; DeLuca, M.; Kilburn, L.; Hibbitts, D. Mechanisms and Kinetics of the Dehydrogenation of C6−C8 Cycloalkanes, Cycloalkenes, and Cyclodienes to Aromatics in H-MFI Zeolite Framework. *ACS Catal.* **2023**, *13*, 99−112.
(22) Chen, J.; Li, J.; Wei, Y.; Yuan, C.; Li, B.; Xu, S.; Zhou, Y.; Wang, J.; Zhang, M.; Liu, Z. Spatial confinement effects of cage-type SAPO molecular sieves on product distribution and coke formation in methanol-to-olefin reaction. *Catal. Commun.* **2014**, *46*, 36−40.
(23) Dai, W.; Wu, G.; Li, L.; Guan, N.; Hunger, M. Mechanisms of the Deactivation of SAPO-34 Materials with Different Crystal Sizes Applied as MTO Catalysts. *ACS Catal.* **2013**, *3*, 588−596.
(24) Martinez-Espin, J. S.; Mortén, M.; Janssens, T. V. W.; Svelle, S.; Beato, P.; Olsbye, U. New insights into catalyst deactivation and product distribution of zeolites in the methanol-to-hydrocarbons (MTH) reaction with methanol and dimethyl ether feeds. *Catal. Sci. Technol.* **2017**, *7*, 2700−2716.
(25) Bjørgen, M.; Olsbye, U.; Kolboe, S. Coke precursor formation and zeolite deactivation: mechanistic insights from hexamethylbenzene conversion. *J. Catal.* **2003**, *215*, 30−44.
(26) Van Speybroeck, V.; De Wispelaere, K.; Van der Mynsbrugge, J.; Vandichel, M.; Hemelsoet, K.; Waroquier, M. First principle chemical kinetics in zeolites: the methanol-to-olefin process as a case study. *Chem. Soc. Rev.* **2014**, *43*, 7326−7357.
(27) Van Speybroeck, V.; Hemelsoet, K.; Joos, L.; Waroquier, M.; Bell, R. G.; Catlow, C. R. A. Advances in theory and their application within the field of zeolite chemistry. *Chem. Soc. Rev.* **2015**, *44*, 7044−7111.
(28) Van Speybroeck, V.; Bocus, M.; Cnudde, P.; Vanduyfhuys, L. Operando Modeling of Zeolite-Catalyzed Reactions Using First-Principles Molecular Dynamics Simulations. *ACS Catal.* **2023**, *13*, 11455−11493.
(29) Chizallet, C.; Bouchy, C.; Larmier, K.; Pirngruber, G. Molecular Views on Mechanisms of Bronsted Acid-Catalyzed Reactions in Zeolites. *Chem. Rev.* **2023**, *123*, 6107−6196.
(30) Haw, J. F.; Song, W.; Marcus, D. M.; Nicholas, J. B. The Mechanism of Methanol to Hydrocarbon Catalysis. *Acc. Chem. Res.* **2003**, *36*, 317−326.
(31) Hemelsoet, K.; Van der Mynsbrugge, J.; De Wispelaere, K.; Waroquier, M.; Van Speybroeck, V. Unraveling the Reaction Mechanisms Governing Methanol-to-Olefins Catalysis by Theory and Experiment. *ChemPhysChem* **2013**, *14*, 1526−1545.
(32) Lesthaeghe, D.; Horré, A.; Waroquier, M.; Marin, G. B.; Van Speybroeck, V. Theoretical Insights on Methylbenzene Side-Chain Growth in ZSM-5 Zeolites for Methanol-to-Olefin Conversion. *Chem.—Eur. J.* **2009**, *15*, 10803−10808.
(33) Yarulina, I.; Bailleul, S.; Pustovarenko, A.; Martinez, J. R.; Wispelaere, K. D.; Hajek, J.; Weckhuysen, B. M.; Houben, K.; Baldus, M.; Van Speybroeck, V.; et al. Suppression of the Aromatic Cycle in Methanol-to-Olefins Reaction over ZSM-5 by Post-Synthetic Modification Using Calcium. *ChemCatChem* **2016**, *8*, 3057−3063.
(34) Yarulina, I.; De Wispelaere, K.; Bailleul, S.; Goetze, J.; Radersma, M.; Abou-Hamad, E.; Vollmer, I.; Goesten, M.; Mezari, B.; Hensen, E. J. M.; et al. Structure−performance descriptors and the role of Lewis acidity in the methanol-to-propylene process. *Nat. Chem.* **2018**, *10*, 804−812.
(35) Bjørgen, M.; Olsbye, U.; Petersen, D.; Kolboe, S. The methanol-to-hydrocarbons reaction: insight into the reaction mechanism from [12C]benzene and [13C]methanol coreactions over zeolite H-beta. *J. Catal.* **2004**, *221*, 1−10.
(36) Wang, C.-M.; Wang, Y.-D.; Xie, Z.-K. Verification of the dual cycle mechanism for methanol-to-olefin conversion in HSAPO-34: a methylbenzene-based cycle from DFT calculations. *Catal. Sci. Technol.* **2014**, *4*, 2631−2638.
(37) Wang, C.-M.; Wang, Y.-D.; Du, Y.-J.; Yang, G.; Xie, Z.-K. Similarities and differences between aromatic-based and olefin-based cycles in H-SAPO-34 and H-SSZ-13 for methanol-to-olefins conversion: insights from energetic span model. *Catal. Sci. Technol.* **2015**, *5*, 4354−4364.
(38) Bleken, F.; Bjørgen, M.; Palumbo, L.; Bordiga, S.; Svelle, S.; Lillerud, K.-P.; Olsbye, U. The Effect of Acid Strength on the Conversion of Methanol to Olefins Over Acidic Microporous Catalysts with the CHA Topology. *Top. Catal.* **2009**, *52*, 218−228.

https://doi.org/10.1021/acs.jpcc.5c07265
J. Phys. Chem. C 2025, 129, 20971−20980

(39) Bjørgen, M.; Svelle, S.; Joensen, F.; Nerlov, J.; Kolboe, S.; Bonino, F.; Palumbo, L.; Bordiga, S.; Olsbye, U. Conversion of methanol to hydrocarbons over zeolite H-ZSM-5: On the origin of the olefinic species. *J. Catal.* **2007**, *249*, 195−207.
(40) Chen, D.; Moljord, K.; Holmen, A. A methanol to olefins review: Diffusion, coke formation and deactivation on SAPO type catalysts. *Microporous Mesoporous Mater.* **2012**, *164*, 239−250.
(41) Bleken, F. L.; Janssens, T. V.; Svelle, S.; Olsbye, U. Product yield in methanol conversion over ZSM-5 is predominantly independent of coke content. *Microporous Mesoporous Mater.* **2012**, *164*, 190−198.
(42) Seo, G.; Kim, J. H.; Jang, H. G. Methanol-to-Olefin Conversion over Zeolite Catalysts: Active Intermediates and Deactivation. *Catal. Surv. Asia* **2013**, *17*, 103−118.
(43) Zachariou, A.; Hawkins, A. P.; Suwardiyanto; Collier, P.; Barrow, N.; Howe, R. F.; Parker, S. F.; Lennon, D. New Spectroscopic Insight into the Deactivation of a ZSM-5 Methanol-to-Hydrocarbons Catalyst. *ChemCatChem* **2021**, *13*, 2625−2633.
(44) Chen, W.; Han, J.; Wei, Y.; Zheng, A. Frustrated Lewis Pair in Zeolite Cages for Alkane Activations. *Angew. Chem., Int. Ed.* **2022**, *61*, No. e202116269.
(45) Li, M.; Ye, Y.; Bai, B.; Liu, C.; Wang, H.; Xu, Z.; Xiao, J.; Jiao, F.; Pan, X.; Bao, X. Zeotype-Confined Frustrated Lewis Pair and Its Role in Catalyzing Hydrogenation. *J. Am. Chem. Soc.* **2025**, *147*, 15747−15754.
(46) Kang, J. H.; Alshafei, F. H.; Zones, S. I.; Davis, M. E. Cage-Defining Ring: A Molecular Sieve Structural Indicator for Light Olefin Product Distribution from the Methanol-to-Olefins Reaction. *ACS Catal.* **2019**, *9*, 6012−6019.
(47) Ferri, P.; Li, C.; Paris, C.; Vidal-Moya, A.; Moliner, M.; Boronat, M.; Corma, A. Chemical and Structural Parameter Connecting Cavity Architecture, Confined Hydrocarbon Pool Species, and MTO Product Selectivity in Small-Pore Cage-Based Zeolites. *ACS Catal.* **2019**, *9*, 11542−11551.
(48) Nesterenko, N.; Aguilhon, J.; Bodart, P.; Minoux, D.; Dath, J. P. *Zeolites and Zeolite-like Materials*; Elsevier Inc., 2016; pp 189−263.
(49) Wang, C.-M.; Wang, Y.-D.; Du, Y.-J.; Yang, G.; Xie, Z.-K. Computational insights into the reaction mechanism of methanol-to-olefins conversion in H-ZSM-5: nature of hydrocarbon pool. *Catal. Sci. Technol.* **2016**, *6*, 3279−3288.
(50) Wang, S.; Chen, Y.; Wei, Z.; Qin, Z.; Ma, H.; Dong, M.; Li, J.; Fan, W.; Wang, J. Polymethylbenzene or Alkene Cycle? Theoretical Study on Their Contribution to the Process of Methanol to Olefins over H-ZSM-5 Zeolite. *J. Phys. Chem. C* **2015**, *119*, 28482−28498.
(51) Chen, Y.; Wang, S.; Wei, Z.; Li, J.; Dong, M.; Qin, Z.; Wang, J.; Fan, W. Unraveling the Relationship between Zeolite Structure and MTO Product Distribution by Theoretical Study of the Reaction Mechanism. *J. Phys. Chem. C* **2021**, *125*, 26472−26483.
(52) Enss, A. E.; Plessow, P. N.; Studt, F. Theoretical investigation of the paring mechanism of the MTO process in different zeolites. *J. Catal.* **2024**, *432*, 115363.
(53) Ke, J.; Hu, W.-D.; Du, Y.-J.; Wang, Y.-D.; Wang, C.-M.; Xie, Z.-K. Microkinetic Simulations of Methanol-to-Olefin Conversion in H-SAPO-34: Dynamic Distribution and Evolution of the Hydrocarbon Pool and Implications for Catalytic Performance. *ACS Catal.* **2023**, *13*, 8642−8661.
(54) Wang, C.-M.; Wang, Y.-D.; Du, Y.-J.; Yang, G.; Xie, Z.-K. Computational insights into the reaction mechanism of methanol-to-olefins conversion in H-ZSM-5: nature of hydrocarbon pool. *Catal. Sci. Technol.* **2016**, *6*, 3279−3288.
(55) Fečík, M.; Plessow, P. N.; Studt, F. Theoretical investigation of the side-chain mechanism of the MTO process over H-SSZ-13 using DFT and ab initio calculations. *Catal. Sci. Technol.* **2021**, *11*, 3826−3833.
(56) Wang, C.-M.; Wang, Y.-D.; Xie, Z.-K.; Liu, Z.-P. Methanol to Olefin Conversion on HSAPO-34 Zeolite from Periodic Density Functional Theory Calculations: A Complete Cycle of Side Chain Hydrocarbon Pool Mechanism. *J. Phys. Chem. C* **2009**, *113*, 4584−4591.
(57) De Wispelaere, K.; Hemelsoet, K.; Waroquier, M.; Van Speybroeck, V. Complete low-barrier side-chain route for olefin formation during methanol conversion in H-SAPO-34. *J. Catal.* **2013**, *305*, 76−80.
(58) Plessow, P. N.; Studt, F. Cooperative Effects of Active Sites in the MTO Process: A Computational Study of the Aromatic Cycle in H-SSZ-13. *ACS Catal.* **2023**, *13*, 624−632.
(59) Haw, J. F.; Nicholas, J. B.; Song, W.; Deng, F.; Wang, Z.; Xu, T.; Heneghan, C. S. Roles for Cyclopentenyl Cations in the Synthesis of Hydrocarbons from Methanol on Zeolite Catalyst HZSM-5. *J. Am. Chem. Soc.* **2000**, *122*, 4763−4775.
(60) Zhang, W.; Zhang, M.; Xu, S.; Gao, S.; Wei, Y.; Liu, Z. Methylcyclopentenyl Cations Linking Initial Stage and Highly Efficient Stage in Methanol-to-Hydrocarbon Process. *ACS Catal.* **2020**, *10*, 4510−4516.
(61) Wang, C.; Chu, Y.; Zheng, A.; Xu, J.; Wang, Q.; Gao, P.; Qi, G.; Gong, Y.; Deng, F. New Insight into the Hydrocarbon-Pool Chemistry of the Methanol-to-Olefins Conversion over Zeolite H-ZSM-5 from GC-MS, Solid-State NMR Spectroscopy, and DFT Calculations. *Chem.—Eur. J.* **2014**, *20*, 12432−12443.
(62) Li, J.; Wei, Y.; Chen, J.; Tian, P.; Su, X.; Xu, S.; Qi, Y.; Wang, Q.; Zhou, Y.; He, Y.; et al. Observation of Heptamethylbenzenium Cation over SAPO-Type Molecular Sieve DNL-6 under Real MTO Conversion Conditions. *J. Am. Chem. Soc.* **2012**, *134*, 836−839.
(63) Wulfers, M. J.; Jentoft, F. C. The Role of Cyclopentadienium Ions in Methanol-to-Hydrocarbons Chemistry. *ACS Catal.* **2014**, *4*, 3521−3532.
(64) Hernandez, E. D.; Manookian, B.; Auerbach, S. M.; Jentoft, F. C. Shape-Selective Synthesis of Alkylcyclopentenyl Cations in Zeolites and Spectroscopic Distinction of Constitutional Isomers. *ACS Catal.* **2021**, *11*, 12893−12914.
(65) Hernandez, E. D.; Jentoft, F. C. Spectroscopic Signatures Reveal Cyclopentenyl Cation Contributions in Methanol-to-Olefins Catalysis. *ACS Catal.* **2020**, *10*, 5764−5782.
(66) Minova, I. B.; Matam, S. K.; Greenaway, A.; Catlow, C. R. A.; Frogley, M. D.; Cinque, G.; Wright, P. A.; Howe, R. F. Elementary Steps in the Formation of Hydrocarbons from Surface Methoxy Groups in HZSM-5 Seen by Synchrotron Infrared Microspectroscopy. *ACS Catal.* **2019**, *9*, 6564−6570.
(67) Zhang, M.; Xu, S.; Wei, Y.; Li, J.; Chen, J.; Wang, J.; Zhang, W.; Gao, S.; Li, X.; Wang, C.; et al. Methanol conversion on ZSM-22, ZSM-35 and ZSM-5 zeolites: effects of 10-membered ring zeolite structures on methylcyclopentenyl cations and dual cycle mechanism. *RSC Adv.* **2016**, *6*, 95855−95864.
(68) Wang, C.; Yi, X.; Xu, J.; Qi, G.; Gao, P.; Wang, W.; Chu, Y.; Wang, Q.; Feng, N.; Liu, X.; et al. Experimental Evidence on the Formation of Ethene through Carbocations in Methanol Conversion over H-ZSM-5 Zeolite. *Chem.—Eur. J.* **2015**, *21*, 12061−12068.
(69) Wang, J.; Wei, Y.; Li, J.; Xu, S.; Zhang, W.; He, Y.; Chen, J.; Zhang, M.; Zheng, A.; Deng, F.; et al. Direct observation of methylcyclopentenyl cations (MCP+) and olefin generation in methanol conversion over TON zeolite. *Catal. Sci. Technol.* **2016**, *6*, 89−97.
(70) Xu, S.; Zheng, A.; Wei, Y.; Chen, J.; Li, J.; Chu, Y.; Zhang, M.; Wang, Q.; Zhou, Y.; Wang, J.; et al. Direct Observation of Cyclic Carbenium Ions and Their Role in the Catalytic Cycle of the Methanol-to-Olefin Reaction over Chabazite Zeolites. *Angew. Chem., Int. Ed.* **2013**, *52*, 11564−11568.
(71) Li, J.; Wei, Y.; Chen, J.; Xu, S.; Tian, P.; Yang, X.; Li, B.; Wang, J.; Liu, Z. Cavity Controls the Selectivity: Insights of Confinement Effects on MTO Reaction. *ACS Catal.* **2015**, *5*, 661−665.
(72) Song, W.; Nicholas, J. B.; Haw, J. F. A Persistent Carbenium Ion on the Methanol-to-Olefin Catalyst HSAPO-34: Acetone Shows the Way. *J. Phys. Chem. B* **2001**, *105*, 4317−4323.
(73) Kozuch, S.; Shaik, S. How to conceptualize catalytic cycles? The energetic span model. *Acc. Chem. Res.* **2011**, *44*, 101−110.
(74) Zhang, W.; Xu, S.; Zhi, Y.; Wei, Y.; Liu, Z. Methylcyclopentenyl cation mediated reaction route in methanol-to-olefins reaction over H-RUB-50 with small cavity. *J. Energy Chem.* **2020**, *45*, 25−30.

https://doi.org/10.1021/acs.jpcc.5c07265
J. Phys. Chem. C 2025, 129, 20971−20980

(75) Zhang, W.; Zhi, Y.; Huang, J.; Wu, X.; Zeng, S.; Xu, S.; Zheng, A.; Wei, Y.; Liu, Z. Methanol to Olefins Reaction Route Based on Methylcyclopentadienes as Critical Intermediates. *ACS Catal.* **2019**, *9*, 7373−7379.
(76) Perdew, J. P.; Burke, K.; Ernzerhof, M. Generalized Gradient Approximation Made Simple. *Phys. Rev. Lett.* **1996**, *77*, 3865−3868.
(77) Grimme, S.; Antony, J.; Ehrlich, S.; Krieg, H. A consistent and accurate ab initio parametrization of density functional dispersion correction (DFT-D) for the 94 elements H-Pu. *J. Chem. Phys.* **2010**, *132*, 154104.
(78) Kresse, G.; Furthmüller, J. Efficient iterative schemes for ab initio total-energy calculations using a plane-wave basis set. *Phys. Rev. B: Condens. Matter Mater. Phys.* **1996**, *54*, 11169−11186.
(79) Kresse, G.; Joubert, D. From ultrasoft pseudopotentials to the projector augmented-wave method. *Phys. Rev. B: Condens. Matter Mater. Phys.* **1999**, *59*, 1758−1775.
(80) Blöchl, P. E. Projector augmented-wave method. *Phys. Rev. B: Condens. Matter Mater. Phys.* **1994**, *50*, 17953−17979.
(81) DeLuca, M.; Kravchenko, P.; Hoffman, A.; Hibbitts, D. Mechanism and Kinetics of Methylating C6−C12 Methylbenzenes with Methanol and Dimethyl Ether in H-MFI Zeolites. *ACS Catal.* **2019**, *9*, 6444−6460.
(82) Fečík, M.; Plessow, P. N.; Studt, F. A Systematic Study of Methylation from Benzene to Hexamethylbenzene in H-SSZ-13 Using Density Functional Theory and Ab Initio Calculations. *ACS Catal.* **2020**, *10*, 8916−8925.
(83) Wen, Z.; Zhu, H.; Zhu, X. Density Functional Theory Study of the Zeolite-Catalyzed Methylation of Benzene with Methanol. *Catal. Lett.* **2020**, *150*, 21−30.
(84) Moors, S. L. C.; De Wispelaere, K.; Van der Mynsbrugge, J.; Waroquier, M.; Van Speybroeck, V. Molecular Dynamics Kinetic Study on the Zeolite-Catalyzed Benzene Methylation in ZSM-5. *ACS Catal.* **2013**, *3*, 2556−2567.
(85) DeLuca, M.; Janes, C.; Hibbitts, D. Contrasting Arene, Alkene, Diene, and Formaldehyde Hydrogenation in H-ZSM-5, H-SSZ-13, and H-SAPO-34 Frameworks during MTO. *ACS Catal.* **2020**, *10*, 4593−4607.
(86) Plessow, P. N. Efficient Transition State Optimization of Periodic Structures through Automated Relaxed Potential Energy Surface Scans. *J. Chem. Theory Comput.* **2018**, *14*, 981−990.
(87) Goncalves, T. J.; Plessow, P. N.; Studt, F. On the Accuracy of Density Functional Theory in Zeolite Catalysis. *ChemCatChem* **2019**, *11*, 4368−4376.
(88) Huber, P.; Plessow, P. N. Accurate and Efficient Description of Acidic Zeolites with Plane-Wave Density Functional Theory Using Range-Separated Hybrid Functionals. *ChemPhysChem* **2025**, *26*, No. e202500147.
(89) Plessow, P. N. Anharmonic Adsorption Free Energies and Apparent Activation Barriers for Mobile Reactants Based on Molecular Dynamics Simulations. *J. Chem. Theory Comput.* **2025**, *21*, 8518−8532.
(90) Mardirossian, N.; Head-Gordon, M. ωB97M-V. A combinatorially optimized, range-separated hybrid, meta-GGA density functional with VV10 nonlocal correlation. *J. Chem. Phys.* **2016**, *144*, 214110.
(91) Najibi, A.; Goerigk, L. DFT-D4 counterparts of leading meta-generalized-gradient approximation and hybrid density functionals for energetics and geometries. *J. Comput. Chem.* **2020**, *41*, 2562−2572.
(92) Najibi, A.; Goerigk, L. The Nonlocal Kernel in van der Waals Density Functionals as an Additive Correction: An Extensive Analysis with Special Emphasis on the B97M-V and ωB97M-V Approaches. *J. Chem. Theory Comput.* **2018**, *14*, 5725−5738.
(93) Deutschmann, O.; Tischer, S.; Kleditzsch, S.; Janardhanan, V.; Correa, C.; Chatterjee, D.; Mladenov, N.; Minh, H. D.; Karadeniz, H.; Hettel, M.; Menon, V.; Banerjee, A.; Gossler, H.; Shirsath, A.; Daymo, E. DETCHEM. 2022, https://www.detchem.com (accessed Nov 04, 2025).
(94) Weitkamp, J.; Jacobs, P. A.; Martens, J. A. Isomerization and hydrocracking of C9 through C16 n-alkanes on Pt/HZSM-5 zeolite. *Appl. Catal.* **1983**, *8*, 123−141.
(95) Plessow, P. N.; Studt, F. Olefin methylation and cracking reactions in H-SSZ-13 investigated with ab initio and DFT calculations. *Catal. Sci. Technol.* **2018**, *8*, 4420−4429.
(96) Brogaard, R. Y.; Henry, R.; Schuurman, Y.; Medford, A. J.; Moses, P. G.; Beato, P.; Svelle, S.; Nørskov, J. K.; Olsbye, U. Methanol-to-hydrocarbons conversion: The alkene methylation pathway. *J. Catal.* **2014**, *314*, 159−169.
(97) Huber, P.; Studt, F.; Plessow, P. N. Reactivity of Surface Lewis and Brønsted Acid Sites in Zeolite Catalysis: A Computational Case Study of DME Synthesis Using H-SSZ-13. *J. Phys. Chem. C* **2022**, *126*, 5896−5905.

https://doi.org/10.1021/acs.jpcc.5c07265
J. Phys. Chem. C 2025, 129, 20971−20980